Asian Journal of Chemistry; Vol. 38, No. 11 (2026), 2929-2937
ASIAN JOURNAL OF CHEMISTRY
https://doi.org/10.14233/ajchem.2026.36807

Design of Co-Modified $NiFe_2O_4$ Spinel Ferrites for Supercapacitor Applications

KHUNDRAKPAM SOMEN SINGH[1], NAVEEN CHANDRA JOSHI[2] and B.S. RAWAT[3,*]

[1]Department of Chemistry, School of Applied & life Sciences, Uttaranchal University, Dehradun-248007, India
[2]Department of Chemistry, Graphic Era (Deemed to be University), Dehradun-248001, India
[3]Department of Physics, Uttaranchal Institute of Technology, Uttaranchal University, Dehradun-248007, India

*Corresponding author: E-mail: park_bhupendra@hotmail.com

Received: 9 July 2026 *Accepted*: 1 October 2026 *Published online*: 13 November 2026 AJC-22524

Spinel ferrites have emerged as promising electrode materials for supercapacitors due to their high theoretical capacitance and fast redox kinetics. In this study, pristine $NiFe_2O_4$ and Co-modified $NiFe_2O_4$ were synthesized *via* a facile, cost-effective and scalable approach, followed by comprehensive structural and electrochemical characterization. Co-modification was associated with enhanced electrochemical performance, which may arise from changes in surface chemistry, redox-active species, morphology and electrode resistance. The $NiFe_2O_4$/200 mg Co electrode exhibited a specific capacitance of 236 F g^{-1} at 2 A g^{-1}, compared with 148 F g^{-1} for pristine $NiFe_2O_4$ under the same measurement conditions. The Co-treated electrode retained approximately 92.1% of its initial capacitance after 5000 charge-discharge cycles in three electrode configuration and 89.3% retention in two-electrode system over the same cycle life. The device delivered a maximum energy density of 6.9 W kg^{-1} and a power density of 4999.2 W kg^{-1}. These electrochemical results establish Co-modified $NiFe_2O_4$ as a promising electrode material for supercapacitor applications.

Keywords: Supercapacitors, Spinel ferrites, Co-modified $NiFe_2O_4$, Electrochemical performance.

INTRODUCTION

The integration of renewable energy sources into decarbonization strategies has increased the need for efficient energy storage systems that support grid stability and ensure reliable power delivery [1-4]. The growing use of wearable devices and portable electronics has also created demand for affordable and lightweight energy storage technologies with high power density and rapid charge–discharge capability [5].

Supercapacitors (SCs) have attracted considerable attention due to their high-power density and excellent cycling stability and their ability to charge and discharge rapidly compared with conventional batteries [6]. Research in this field has focused on improving electrode materials based on transition metal oxides and ferrites along with their composites through suitable synthesis methods and electrolyte optimization [7]. Transition metal oxides and ferrites are widely studied as electrode materials due to their redox-active sites facilitate Faradaic charge storage [8]. Bimetallic ferrites offer multiple oxidation states and enhanced redox activity, which can improve their charge storage performance [9]. For example, $NiFe_2O_4$ thin films prepared by spray pyrolysis have exhibited a specific capacitance of 600 F g^{-1} [10] whereas hydrothermally synthesized $NiFe_2O_4$ has shown a value of 266 F g^{-1} [11]. Such differences highlight the influence of synthesis conditions and surface morphology on electrochemical performance. Structural modification and metal-ion doping have also been investigated as strategies to improve the charge storage capability and cycling stability of $NiFe_2O_4$ electrodes [12]. Nickel ferrite has received particular interest for supercapacitors and other applications such as water purification and catalysis. Its electrochemical performance can be further improved through the incorporation of conductive materials or suitable metal dopants [10]. Cobalt is of interest in this context since its redox activity can contribute to pseudo-capacitive charge storage and improved electrical transport [13].

Despite these advantages the relatively low electrical conductivity of $NiFe_2O_4$ remains a limitation for supercapacitor applications. Nanostructuring and surface engineering and partial substitution with other transition metal ions have been explored to address this issue [14-16]. Cobalt containing ferrite composites have shown improved pseudocapacitive behaviour through enhanced redox activity and charge transport [17,18]. For example, $NiFe_2O_4$-$CoFe_2O_4$ composites have

This is an open access journal, and articles are distributed under the terms of the Attribution 4.0 International (CC BY 4.0) License. This license lets others distribute, remix, tweak, and build upon your work, even commercially, as long as they credit the author for the original creation. You must give appropriate credit, provide a link to the license, and indicate if changes were made.

been reported to deliver a specific capacitance of 800 F g^{-1} while retaining 85% of their initial capacitance after 10,000 cycles [19].

Although $NiFe_2O_4$-based materials have been widely investigated for supercapacitor applications systematic studies of Co-modified $NiFe_2O_4$ prepared through simple and scalable synthesis routes remain limited particularly those comparing electrochemical performance in both three-electrode and two-electrode configurations. In this study, Co modification of preformed $NiFe_2O_4$ was investigated to examine its effects on structural and morphological characteristics and electrochemical performance. Materials with different cobalt concentrations were prepared using straightforward and cost-effective methods. The optimized electrode was further evaluated in a two-electrode configuration to assess its practical energy storage performance and cycling stability.

EXPERIMENTAL

All chemicals were of AR grade and used without further purification. Nickel nitrate hexahydrate [$Ni(NO_3)_2{\cdot}6H_2O$], ferric nitrate hexahydrate [$Fe(NO_3)_3$], cobalt nitrate hexahydrate [$Co(NO_3)_2{\cdot}6H_2O$], sodium hydroxide, N-methyl-2-pyrrolidone (NMP), citric acid, carbon black, polyvinylidene fluoride (PVDF) were used. Acetone and double distilled water were used as solvents during synthesis and electrode preparation.

Synthesis of $NiFe_2O_4$ and Co-Modified $NiFe_2O_4$: $NiFe_2O_4$ spinel ferrite was synthesized through a simple solution-based method. Initially, 0.5 g of $Ni(NO_3){\cdot}6H_2O$ and 1 g of $Fe(NO_3)$ were dissolved in 100 mL of double distilled water under continuous stirring for 35 min to obtain a homogeneous solution. Subsequently, 500 mg of citric acid was added as a complexing agent and the solution was further stirred for 35 min to ensure uniform complex formation between the metal ions. To facilitate precipitation, a few drops of 0.1 M NaOH solution were added gradually under continuous stirring for 60 min to adjust the pH and facilitate the formation of the corresponding metal hydroxide precursor. The resulting suspension was centrifuged and the precipitate was collected and washed several times with double-distilled water to remove residual impurities. The washed precipitate was then dried in a hot air oven and subsequently calcined at 650 ºC for 3.5 h to obtain crystalline $NiFe_2O_4$. Subsequently, the preformed $NiFe_2O_4$ was subjected to Co treatment using two different amounts of cobalt precursor (100 and 200 mg). The required amount of $Co(NO_3)_2{\cdot}6H_2O$ was mixed separately with 100 mg of the synthesized $NiFe_2O_4$ powder. Each mixture was mechanically ground for 1 h to promote uniform distribution of the cobalt-containing species followed by ultrasonication for 2 h to improve dispersion. The resulting mixtures were dried and subsequently calcined at 650 ºC. The resulting materials are designated as $NiFe_2O_4$/100 mg Co and $NiFe_2O_4$/200 mg Co, respectively and are referred to as Co-modified $NiFe_2O_4$. In this study, the modification level is expressed in terms of the Co precursor loading rather than the actual Co content or a specific Co substitution level in the $NiFe_2O_4$ lattice. The samples were stored in airtight containers for further characterization.

Electrochemical studies: The electrode slurry was prepared by combining 10 mg of PVDF, 10 mg of carbon black and 80 mg of $NiFe_2O_4$ or Co-modified $NiFe_2O_4$ in the presence of NMP. After that, a resulting slurry was applied on Ni-foam and dried at 80 ºC for 6 h. Acetone and double distilled water were used to wash the Ni-foam prior to coating. The obtained electrode was used as the working electrode, while the Ag/AgCl electrode was used as the reference electrode with the Pt electrode (counter electrode). Electrochemical studies were conducted in the presence of 1 M KOH solution. The electrode capabilities have been investigated using cyclic voltammetry (CV), capacity retention, electrochemical impedance spectroscopy (EIS) and galvanostatic charge-discharge (GCD), respectively.

RESULTS AND DISCUSSION

FTIR analysis: The FTIR spectra (Fig. 1) were analyzed to identify the functional groups and metal–oxygen bonds in the synthesized spinel ferrites. Pristine $NiFe_2O_4$ exhibited absorption bands at 3471 and 1636 cm^{-1}, which is assigned to the O–H stretching and bending vibrations of surface hydroxyl groups and adsorbed water molecules. Such bands are commonly observed in the spinel ferrite nanoparticles [20].

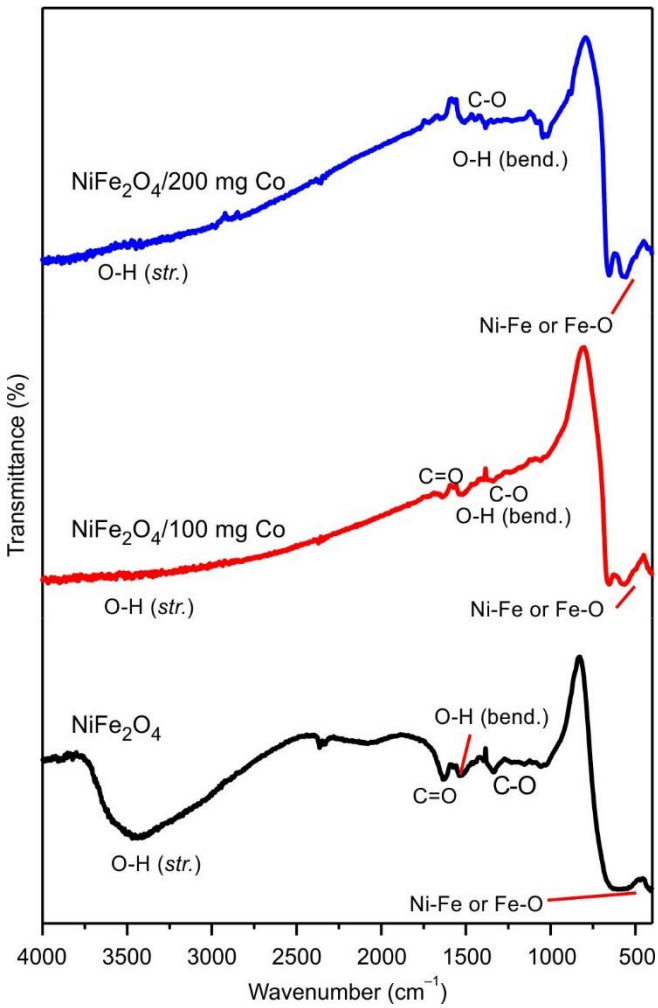


Fig. 1. FTIR spectra of $NiFe_2O_4$, $NiFe_2O_4$/100 mg Co and $NiFe_2O_4$/200 mg Co

The absorption band near 605 cm^{-1} is attributed to M–O vibrations associated with the ferrite lattice. These vibrations generally occur in the 600-400 cm^{-1} region and are characteristic of spinel ferrites [21,22].

The bands at 1553 and 1337 cm^{-1} may be associated with O–H bending and C–O stretching vibrations arising from surface species or residual organic compounds from the synthesis process [23]. The $NiFe_2O_4$/100 mg Co composite exhibited absorption bands at 3437, 1537, 1340, 654 and 562 cm^{-1}. The bands at 654 and 562 cm^{-1} fall within the characteristic M–O vibration region of ferrite materials [24,25]. For the $NiFe_2O_4$/200 mg Co composite, the main absorption bands appeared at 3447, 1535, 666 and 557 cm^{-1}. These bands are assigned to O–H stretching and bending vibrations and M–O vibrations associated with the ferrite framework [26-32].

Small shifts in the absorption bands were observed after Co treatment. These changes may arise from variations in the local chemical environment and metal–oxygen interactions. The bands in the 700-400 cm^{-1} region provide the main FTIR evidence for M–O bonding in the spinel ferrite framework, whereas the higher-wavenumber bands are primarily associated with surface hydroxyl groups and adsorbed water. The observed spectral changes are consistent with modifications in the surface or local bonding environment after Co treatment.

XRD analysis: Fig. 2 shows the XRD patterns of pristine $NiFe_2O_4$ and Co-modified $NiFe_2O_4$ samples. Pristine $NiFe_2O_4$ exhibits characteristic diffraction peaks at $2\theta \approx 30.5^o$, 35.6^o, 43.5^o, 53.8^o, 57.3^o and 62.8^o, corresponding to the (220), (311), (400), (422), (511) and (440) planes of the cubic spinel structure. These reflections agree with JCPDS card No. 10-0325 [33]. The principal $NiFe_2O_4$ reflections remain visible in the samples treated with 100 and 200 mg of Co. The changes in peak intensity and broadening suggest variations in crystallinity and microstructural characteristics after Co treatment. The crystallite sizes estimated from peak broadening range from 0.53 to 38.60 nm, with an arithmetic mean of approximately 11.91 nm. The weak additional diffraction peaks appear in the Co-treated samples and are assigned to cubic spinel Co_3O_4 according to JCPDS card No. 42-1467. These reflections indicate the presence of a separate crystalline Co_3O_4 phase alongside the $NiFe_2O_4$ phase. The XRD results support the formation of a Co-modified $NiFe_2O_4$ composite rather than confirming the formation of a single-phase $Ni_{1-x}Co_xFe_2O_4$ solid solution [34-39]. The retention of the main $NiFe_2O_4$ reflections confirms that the parent spinel phase remains detectable after Co treatment, while the additional Co_3O_4 peaks and changes in diffraction profiles point to modifications in the phase composition and microstructure.

Morphological analysis: The surface morphology of pristine $NiFe_2O_4$ and Co-modified $NiFe_2O_4$ samples was examined by scanning electron microscopy (SEM), as shown in Fig. 3a-f. Pristine $NiFe_2O_4$ exhibits irregularly shaped and agglomerated particles, a common feature of ferrite nanoparticles prepared by solution-based methods due to magnetic interactions and high surface energy [21,40]. After Co treatment, changes in particle morphology and distribution were observed. The $NiFe_2O_4$/200 mg Co sample exhibits predominantly spherical to semi-spherical particles with a comparatively more uniform distribution. These changes may be associated with surface modification and particle interactions during grinding, sonication, drying and calcination. Such morphological features may influence electrochemical performance by affecting the accessible surface area and electrolyte transport [41]. The energy-dispersive X-ray spectroscopy (EDX) profiles in Fig. 4 confirm the presence of Co in the treated samples. Since EDX is a semi-quantitative technique that provides localized elemental information, the detection of Co does not establish its substitution at Ni^{2+} sites within the $NiFe_2O_4$ lattice.

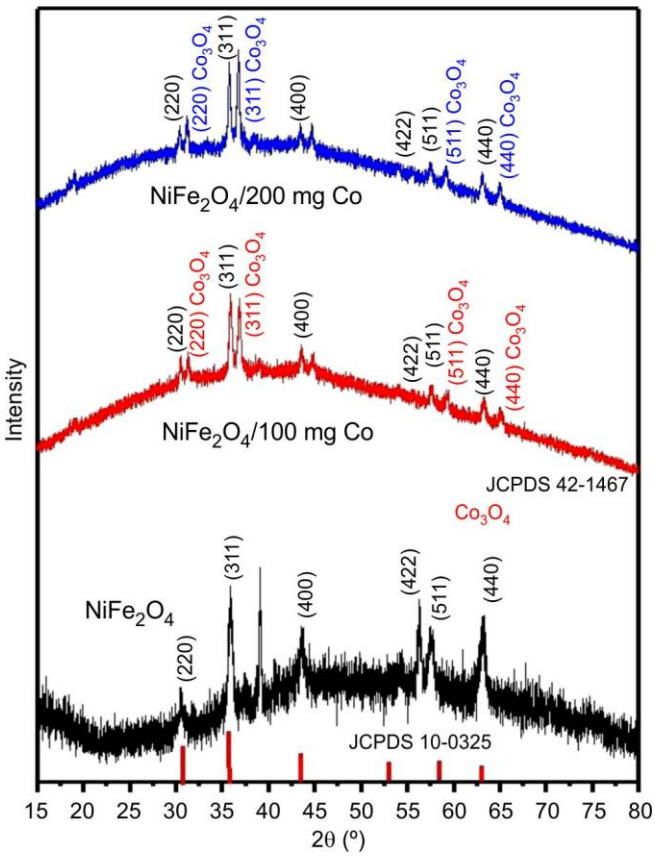


Fig. 2. XRD patterns of $NiFe_2O_4$, $NiFe_2O_4$/100 mg Co and $NiFe_2O_4$/200 mg Co

Transmission electron microscopy (TEM) images of $NiFe_2O_4$/200 mg Co (Fig. 5) further reveal spherical to semi-spherical particles with some degree of agglomeration, which is commonly observed in nanoscale ferrite materials [42,43]. The combined SEM, EDX and TEM results confirm the presence of Co in the treated material and reveal changes in particle morphology and aggregation. These observations support the formation of a Co-modified $NiFe_2O_4$ material but do not independently establish Co incorporation into the ferrite lattice.

Electrochemical study of $NiFe_2O_4$ and Co-incorporated $NiFe_2O_4$

CV analysis: The electrochemical performance of pristine $NiFe_2O_4$ and Co-modified $NiFe_2O_4$ samples containing 100 and 200 mg of Co was investigated using three-electrode and two-electrode configurations. Figs. 6a-d presents the cyclic

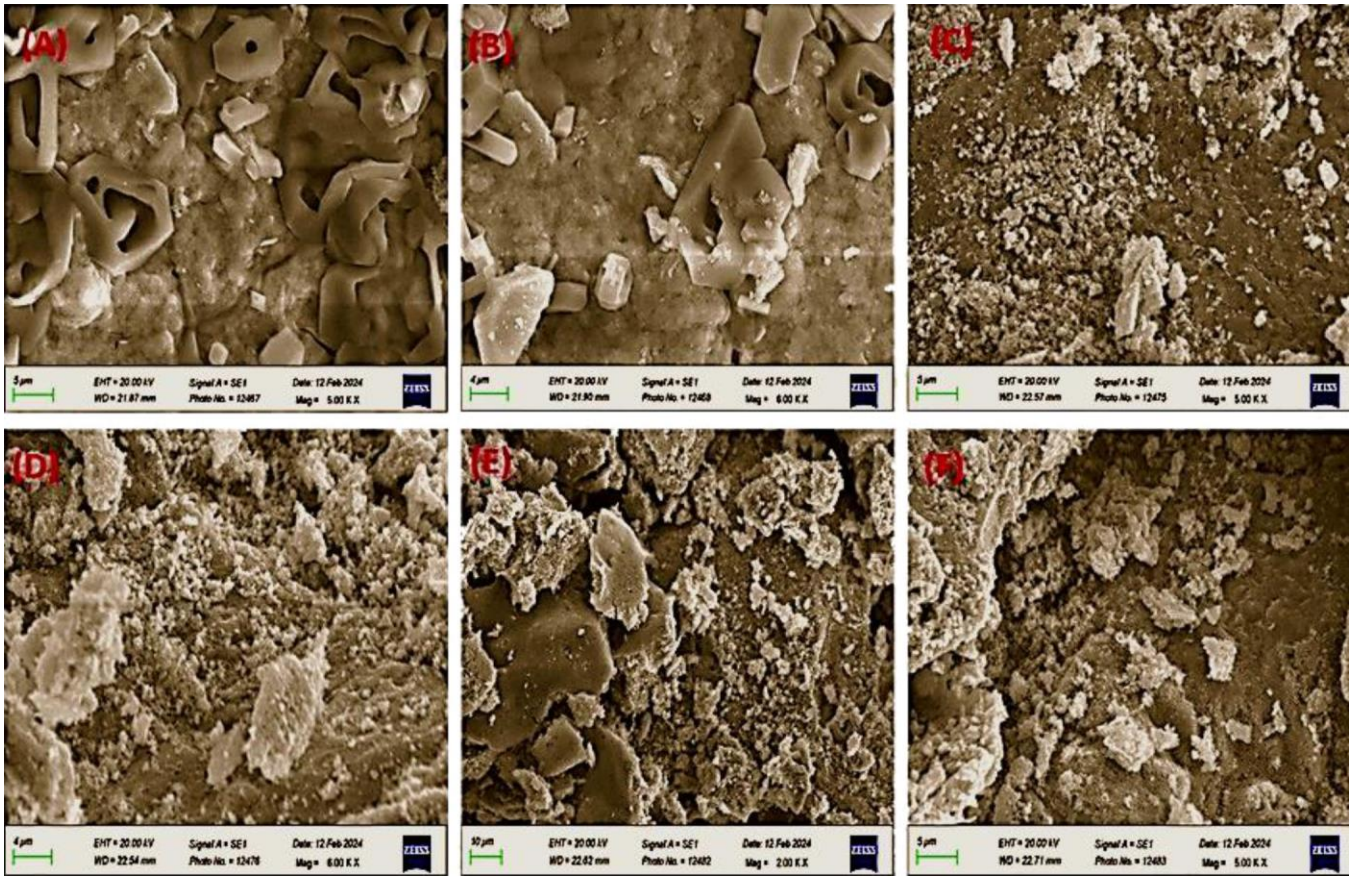


Fig. 3. SEM images of (A-B) pristine $NiFe_2O_4$, (C-D) $NiFe_2O_4$/100 mg Co, (E-F) $NiFe_2O_4$/200 mg Co

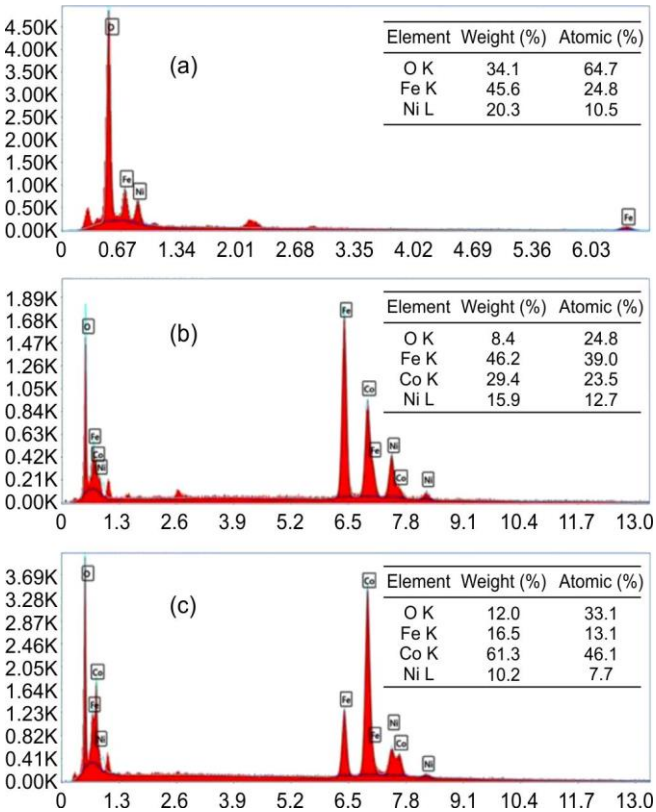


Fig. 4. EDX spectra along with the elemental composition of (a) pristine $NiFe_2O_4$, (b) $NiFe_2O_4$/100 mg Co and (c) $NiFe_2O_4$/200 mg Co

voltammetry (CV) curves recorded at different scan rates. The potential window of −0.5 to +0.5 V was selected to examine the charge-storage behaviour of the electrodes under the applied measurement conditions. CV analysis provides information on redox activity and charge-storage characteristics [44].

Differences in the CV profiles were observed between the two configurations. The three-electrode system, comprising Ag/AgCl as the reference electrode and Pt as the counter electrode, allows the intrinsic electrochemical response of the working electrode to be evaluated. In the two-electrode system, both electrodes contribute to charge storage and the measured response is influenced by device-level factors such as internal resistance, electrode polarization and ion transport [45].

The CV curves exhibit quasi-rectangular profiles with broad Faradaic features across the investigated scan rates. The Co-modified $NiFe_2O_4$ electrode containing 200 mg of Co retains similar redox features in both configurations (Fig. 6c-d), which indicate comparable charge-storage characteristics under the tested conditions. The broad redox features may arise from overlapping Faradaic reactions involving Ni-, Fe- and Co-containing surface species in the alkaline electrolyte. These reactions may involve Ni^{2+}/Ni^{3+} and Co^{2+}/Co^{3+} redox transitions.

Co treatment alters the electrochemical response of $NiFe_2O_4$ and may influence charge transport through changes in surface chemistry and the availability of electrochemically

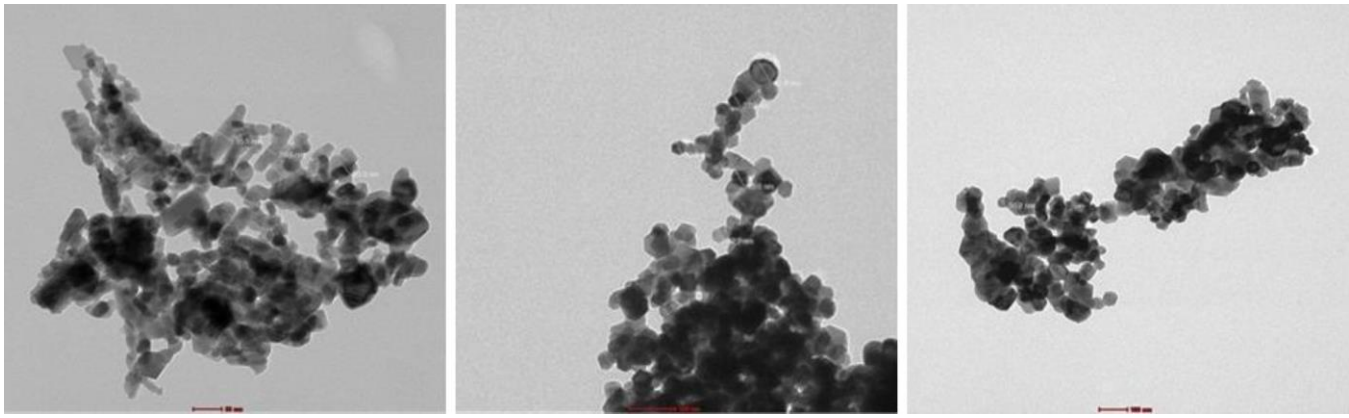


Fig. 5. TEM images of $NiFe_2O_4$/200 mg Co

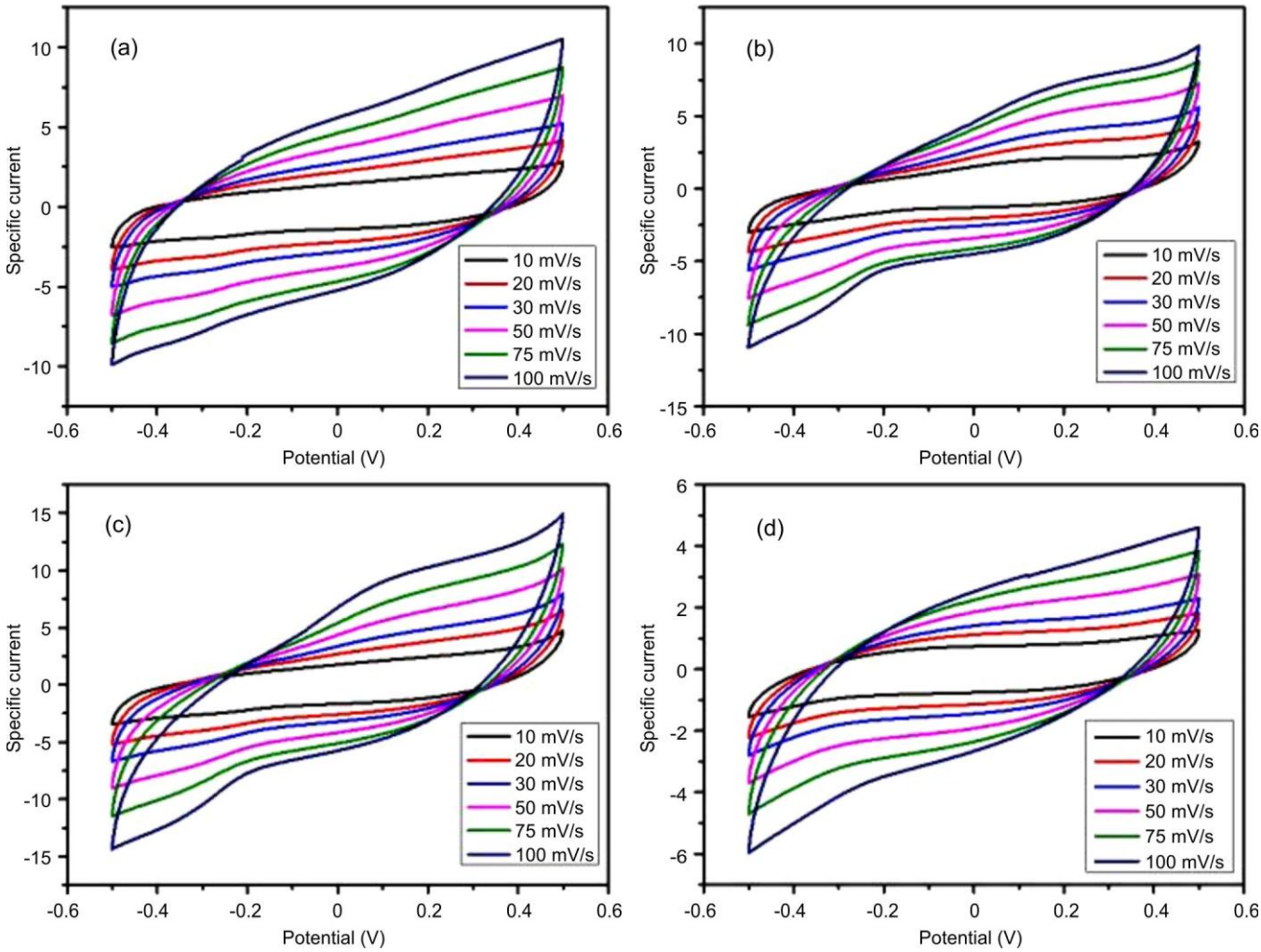


Fig. 6. CV curves of (a) $NiFe_2O_4$, (b) $NiFe_2O_4$/100 mg Co and (c) $NiFe_2O_4$/200 mg Co under three electrode system, (d) $NiFe_2O_4$/200 mg Co under two electrode system

active sites. Variations in particle morphology and electrode–electrolyte interactions may further affect ion accessibility and charge-storage performance. These factors may contribute to the enhanced specific capacitance of the Co-modified electrode [46-48]. Further evidence is required to establish the specific contributions of conductivity changes and individual redox couples to the observed electrochemical improvement.

GCD analysis: Figs. 7a-d presents the galvanostatic charge–discharge (GCD) profiles of pristine $NiFe_2O_4$ and Co-modified $NiFe_2O_4$ containing 100 and 200 mg of Co under three-electrode and two-electrode configurations. The charge storage in the Co-modified electrode may involve Faradaic reactions of Ni- and Co-containing species in the alkaline electrolyte alongside electrical double-layer contributions at

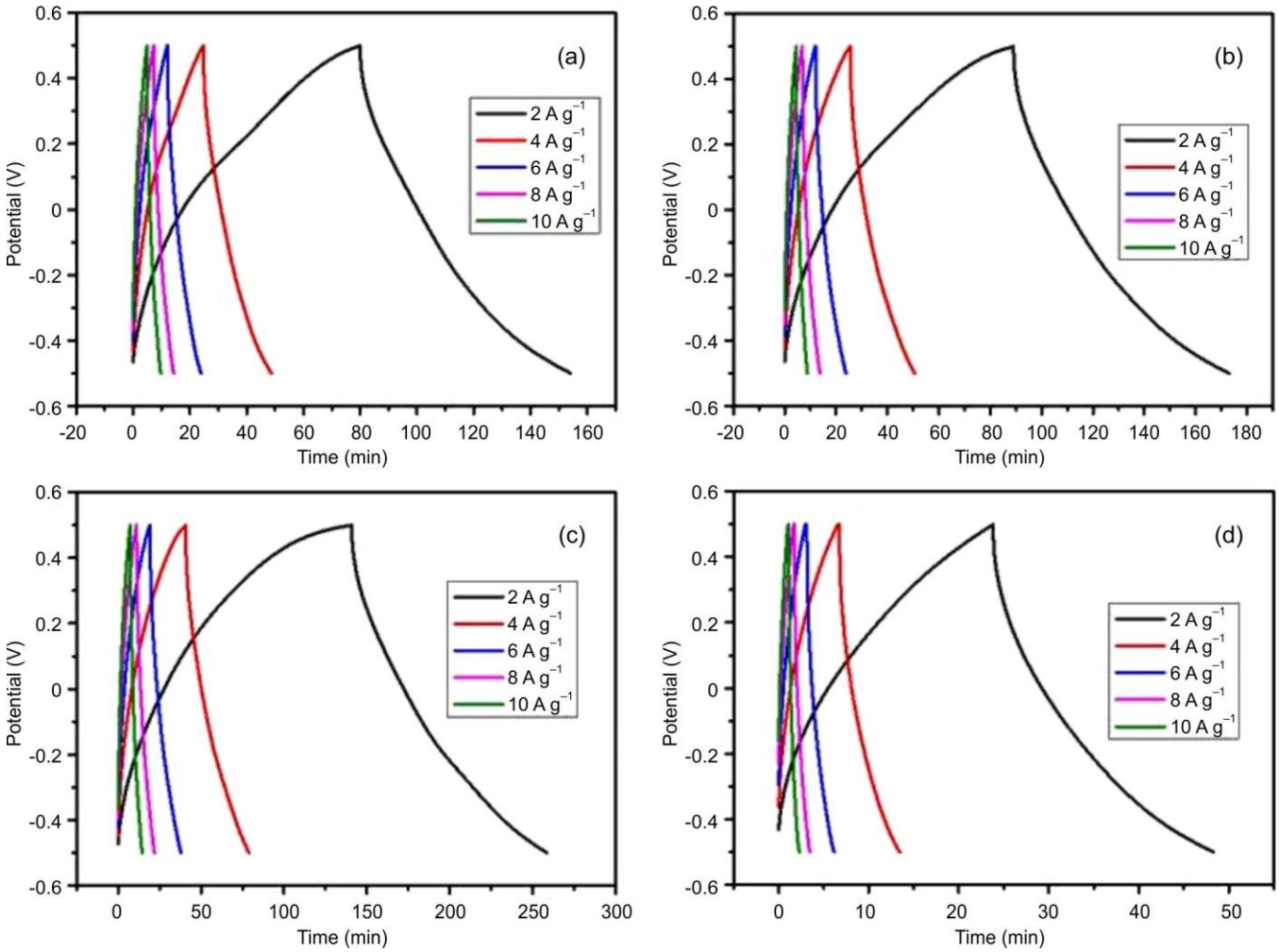


Fig. 7. GCD curves of (a) $NiFe_2O_4$, (b) $NiFe_2O_4$/100 mg Co and (c) $NiFe_2O_4$/200 mg Co under three electrode system, (d) $NiFe_2O_4$/200 mg Co under two electrode system

the electrode-electrolyte interface. The changes in surface chemistry and particle morphology may influence the availability of active sites and electrolyte ion transport [49].

Under the three-electrode configuration (Fig. 8a) the specific capacitance of pristine $NiFe_2O_4$ was 148, 48, 22, 14 and 10 F g^{-1} at current densities of 2, 4, 6, 8 and 10 A g^{-1}, respectively. $NiFe_2O_4$/100 mg Co exhibited values of 170, 52, 26, 16 and 12 F g^{-1} under the same conditions. The highest values were obtained for $NiFe_2O_4$/200 mg Co at 236, 76, 36, 22 and 16 F g^{-1}. In the two-electrode configuration, a symmetric device was assembled using two identical $NiFe_2O_4$/200 mg Co electrodes coated on Ni foam. Without a reference electrode, the measurements represented the full cell voltage response. The device exhibited specific capacitances of 50, 28, 24, 20 and 15 F g^{-1} at current densities of 2, 4, 6, 8 and 10 A g^{-1}, respectively (Fig. 8b).

At 2 A g^{-1}, the Co-modified electrode delivered 236 F g^{-1} compared with 148 F g^{-1} for pristine $NiFe_2O_4$, which represent an increase of approximately 59.5%. The specific capacitance decreased with increasing current density, which may be attributed to restricted ion diffusion and incomplete utilization of electrochemically active sites during rapid charge–discharge. At lower current densities, ions have more time to access the electrode surface and internal active sites. Higher current densities can limit ion transport and increase polarization and thus reduce the effective contribution of the electrode material to charge storage. Despite this decrease, $NiFe_2O_4$/200 mg Co retained a capacitance of 16 F g^{-1} at 10 A g^{-1} in the three-electrode configuration and 15 F g^{-1} in the two-electrode device. The improved capacitance following Co treatment may be associated with changes in redox activity and electrode–electrolyte interactions [50].

Retention, energy and power densities analysis: The $NiFe_2O_4$/200 mg Co electrode retained 99.1% of its initial capacitance after 500 GCD cycles and 97.5% after 2000 cycles in the three-electrode configuration. The capacitance retention remained at 93.2% after 4000 cycles and 92.1% after 5000 cycles. In the two-electrode configuration, the electrode retained 96.3% of its initial capacitance after 500 cycles and 94.2% after 2000 cycles with 89.3% retention after 5000 cycles (Fig. 8c). These results indicate good cycling stability under both configurations.

The symmetric two-electrode device delivered energy densities of 6.9, 3.9, 3.4, 2.8 and 2.1 Wh kg^{-1} at corresponding power densities of 999.9, 1999.5, 2999.7, 3998.8 and 4999.2 W kg^{-1} (Table-1). A comparison with previously

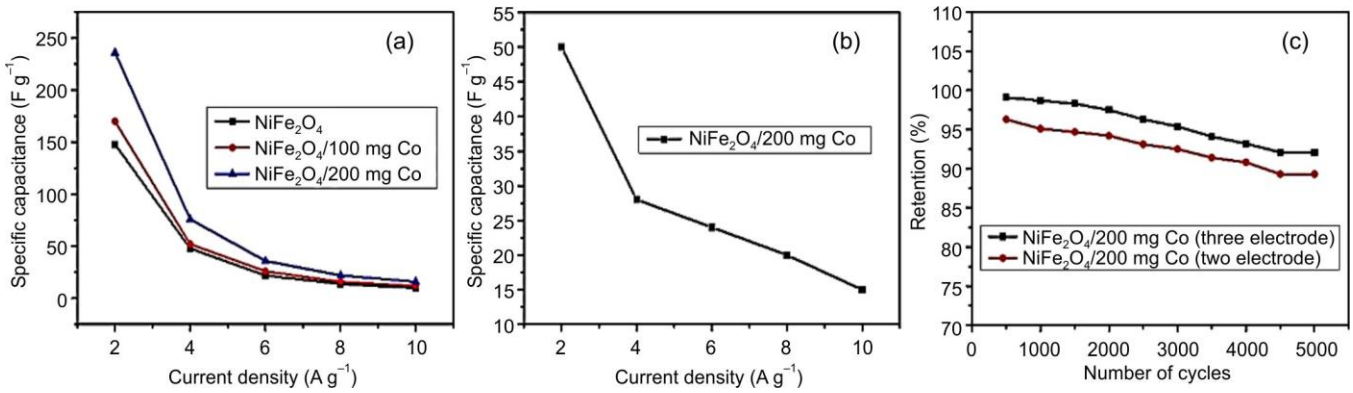


Fig. 8. Plots of (a) specific capacitance *vs*. current density under three electrode system, (b) specific capacitance *vs*. current density under two electrode system and (c) cyclic stability

TABLE-1
ENERGY AND POWER DENSITIES DATA OF $NiFe_2O_4$/200 mg Co

Energy density (Wh kg^{-1})	Power density (W kg^{-1})
6.9	999.9
3.9	1999.5
3.4	2999.7
2.8	3998.8
2.1	4999.2

reported Ni–Co ferrite electrodes is provided in Table-2. The hydrothermally synthesized $Ni_{0.5}Co_{0.5}Fe_2O_4$ exhibited a specific capacitance of 522.80 F g^{-1} at 2.25 A g^{-1} [51] while solvent free-synthesized $Ni_{0.4}Co_{0.6}Fe_2O_4$ delivered 237 F g^{-1} at 1 A g^{-1} [52]. Higher capacitance values have also been reported for compositionally controlled $Ni_{1-x}Co_xFe_2O_4$ systems [53]. Direct comparisons require consideration of differences in the current density and electrolyte composition and electrode configuration and active-material loading. Therefore, the present study does not establish superior performance over previously reported Ni–Co ferrites. Instead, the improvement observed relative to pristine $NiFe_2O_4$ under identical experimental conditions demonstrates the beneficial effect of the present Co-treatment approach on charge-storage performance.

EIS analysis: In present study, $NiFe_2O_4$, $NiFe_2O_4$/100 mg Co and $NiFe_2O_4$/200 mg Co electrodes were analyzed using Nyquist and Bode plots. The Nyquist plots along with their corresponding equivalent circuit models are shown in Fig. 9, while the Bode plots are shown in Fig. 10. The electrochemical parameters extracted from the equivalent circuit fitting include the series resistance (R_s), charge transfer resistance (R_{ct}) and Warburg diffusion element (Z_w). For pristine $NiFe_2O_4$, the values of R_s, R_{ct} and Z_w were found to be 4.464 Ω, 1.015×10^{-2} Ω and 4.87×10^{-7}, respectively. For the $NiFe_2O_4$/100 mg Co electrode, these values were 4.466 Ω, 1.043×10^{-2} and 1.70×10^{-3}, respectively, whereas for $NiFe_2O_4$/200 mg Co they were 3.387 Ω, 1.664×10^{-2} Ω and 4.51×10^{-3}, respectively. The series resistance (R_s) decreases from 4.466 Ω for pristine $NiFe_2O_4$ to 3.387 Ω for $NiFe_2O_4$/200 mg Co, suggesting reduced ohmic resistance within the electrode/electrolyte system. In contrast, the charge transfer resistance (R_{ct}) increases from 1.015×10^{-2} to 1.664×10^{-2} Ω upon increasing the Co treatment, which indicate that the improvement in the electrochemical performance cannot be attributed solely to faster interfacial charge-transfer kinetics. The enhanced capacitance may be attributed to the changes in surface chemistry and morphology and improved accessibility of electroactive sites. EIS analysis indicates lower series resistance but does not directly confirm faster charge-transfer kinetics. The changes in the Warburg parameter suggest modified diffusion-related impedance, whereas Bode plots support the equivalent-circuit analysis and indicate coupled charge-transfer and ion-diffusion processes [49,54].

Conclusion

In this study, pristine $NiFe_2O_4$ and Co-modified $NiFe_2O_4$ materials were synthesized and evaluated as electrode materials for the supercapacitor applications. Structural and morphological analysis confirmed the formation of crystalline spinel ferrite with changes in particle morphology following

TABLE-2
COMPARISON OF THE ELECTROCHEMICAL PERFORMANCE OF
Co-MODIFIED $NiFe_2O_4$ WITH REPORTED Ni-Co FERRITE ELECTRODES

Material	Synthesis	Current density (A g^{-1})	Specific capacitance (F g^{-1})	Cyclic stability	Ref.
$NiFe_2O_4$	Hydrothermal	0.25	467.43	–	[51]
$Ni_{0.5}Co_{0.5}Fe_2O_4$	Hydrothermal	0.25	522.80	82%, 1500	[51]
$CoFe_2O_4$	Hydrothermal	0.25			[51]
$Ni_{0.4}Co_{0.6}Fe_2O_4$	Solventless	1.00	237.00	100%, 4000	[52]
$Ni_{0.5}Co_{0.5}Fe_2O_4$	Auto-combustion	–	996.00	90%, 5000	[53]
$NiFe_2O_4$/200 mg Co	Co treatment of performed $NiFe_2O_4$	2.00	236.00	92.1% after 5000 cycles	Present work

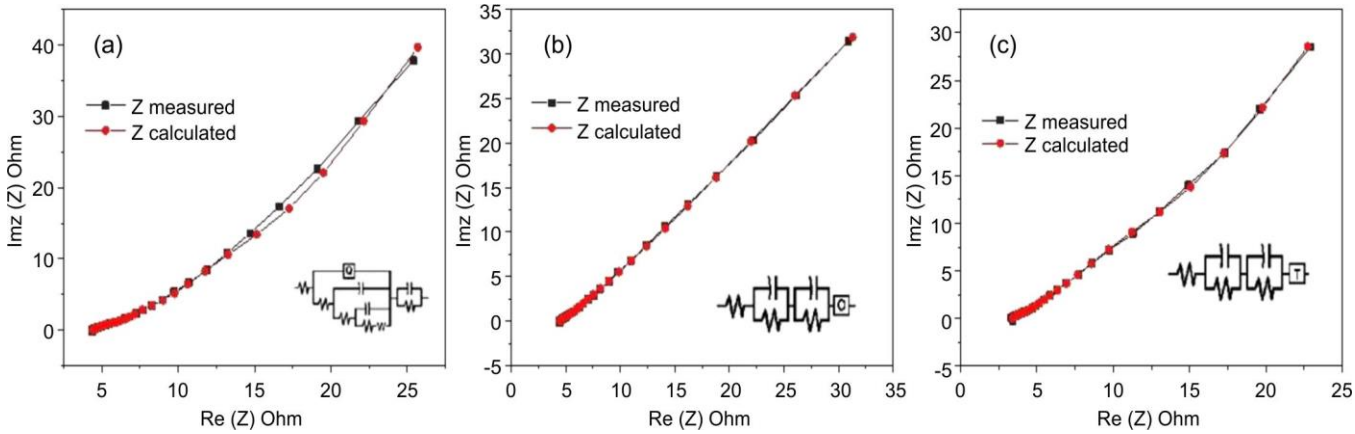


Fig. 9. Nyquist curves of (a) $NiFe_2O_4$, (b) $NiFe_2O_4$/100 mg Co and (c) $NiFe_2O_4$/200 mg Co

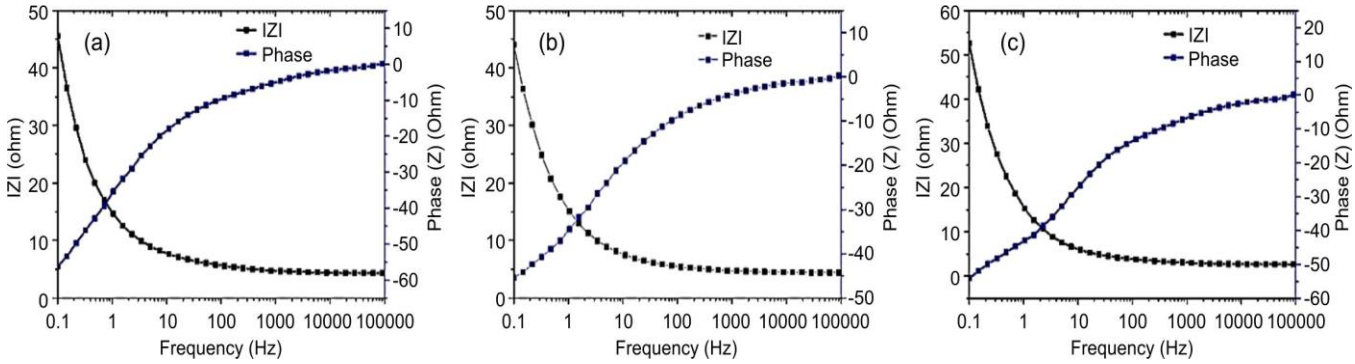


Fig. 10. Bode's curves of (a) $NiFe_2O_4$, (b) $NiFe_2O_4$/100 mg Co and (c) $NiFe_2O_4$/200 mg Co

Co treatment. Electrochemical studies revealed that Co doping enhanced the charge-storage performance of $NiFe_2O_4$. The improvement may be associated with change in surface chemistry and morphology, the contribution of Co-containing redox-active species and the lower series resistance observed for the 200 mg Co-modified electrode. As a result, the specific capacitance increased from 148 to 236 F g^{-1}, with the $NiFe_2O_4$/200 mg Co electrode delivering the highest capacitance of 236 F g^{-1} at a current density of 2 A g^{-1}. Furthermore, the electrode exhibited remarkable cyclic stability, retaining 92.1% of its capacitance after 5000 GCD cycles. When evaluated in a two-electrode device configuration, the $NiFe_2O_4$/200 mg Co electrode maintained 89.3% capacitance retention after 5000 GCD cycles, which signify its promising potential for the practical energy storage applications.

CONFLICT OF INTEREST

The authors declare that there is no conflicts of interest regarding the publication of this article.

DECLARATION OF AI-ASSISTED TECHNOLOGIES

During the preparation of this manuscript, the authors used an AI-assisted tool(s) to improve the language and no data, results or scientific conclusions were generated by AI. All analyses, interpretations and conclusions are the authors' own. The authors reviewed and edited the content and take full responsibility for the published work.

REFERENCES

1. M. Amir, R.G. Deshmukh, H.M. Khalid, Z. Said, S.M. Muyeen, A. Raza, A.S. Nizami, R.M. Elavarasan, R. Saidur and K. Sopian, *J. Energy Storage*, **72**, 108694 (2023); https://doi.org/10.1016/j.est.2023.108694
2. Y. Wu, Y. Deng, J. Zhang, S. Lv, Z. Xiao, L. Liu, X. Jia, C. Chen, Z. Dang, L. Li and L. Wang, *Chem. Eng. J.*, **455**, 140953 (2023); https://doi.org/10.1016/j.cej.2022.140953
3. X. Wang, H. Ding, W. Luo, Y. Yu, Q. Chen, B. Luo, M. Xie and X. Guo, *EcoEnergy*, **1**, 448 (2023); https://doi.org/10.1002/ece2.21
4. D. Sun, Z. Sun, D. Yang, X. Jiang, J. Tang and X. Wang, *EcoEnergy*, **1**, 375 (2023); https://doi.org/10.1002/ece2.22
5. B.-H. Xiao, K. Xiao, J.-X. Li, C.-F. Xiao, S. Cao and Z.-Q. Liu, *Chem. Sci. (Camb.)*, **15**, 11229 (2024); https://doi.org/10.1039/D4SC02139H
6. K. Dissanayake and D. Kularatna-Abeywardana, *J. Energy Storage*, **96**, 112563 (2024); https://doi.org/10.1016/j.est.2024.112563
7. F. Ahmad, A. Shahzad, M. Danish, M. Fatima, M. Adnan, S. Atiq, M. Asim, M.A. Khan, Q.U. Ain and R. Perveen, *J. Energy Storage*, **81**, (2024); https://doi.org/10.1016/j.est.2024.110430
8. R. Liang, Y. Du, P. Xiao, J. Cheng, S. Yuan, Y. Chen, J. Yuan and J. Chen, *Nanomaterials*, **11**, 1248 (2021); https://doi.org/10.3390/nano11051248
9. H.R. Ahmed and A.M. Elias, *Chem. Pap.*, **80**, 9891 (2026); https://doi.org/10.1007/s11696-026-04889-0
10. V.A. Jundale, D.A. Patil and A.A. Yadav, *Phase Transit.*, **95**, 786 (2022); https://doi.org/10.1080/01411594.2022.2122825
11. X.C. Gao, J.Q. Bi, W.L. Wang, G.X. Sun, X.X. Hao, W.K. Yan and L. Wang, *Diffus. Defect Data Solid State Data B Solid State Phenom.*, **281**, 854 (2018); https://doi.org/10.4028/www.scientific.net/SSP.281.854

12. M.B. Askari, P. Salarizadeh and M.T. Tourchi Moghadam, *Fuel*, **403**, 136104 (2026); https://doi.org/10.1016/j.fuel.2025.136104
13. V.D. Patil, D.A. Patil, A.L. Jadhav, S.L. Jadhav, A.V. Kadam, S.R. Dandwate and B.R. Shinde, *Discover Electrochem.*, **1**, 2 (2024); https://doi.org/10.1007/s44373-024-00003-9
14. D. Chu, X. Zhao, B. Xiao, A. Libanori, Y. Zhou, L. Tan, H. Ma, H. Pang, X. Wang, Y. Jiang and J. Chen, *Chem. Eur. J.*, **27**, 8337 (2021); https://doi.org/10.1002/chem.202100265
15. Z. Lv, Q. Zhong, Y. Bu and J. Wu, *Electron. Mater. Lett.*, **12**, 824 (2016); https://doi.org/10.1007/s13391-016-6188-9
16. Y.-Y. Huang and L.-Y. Lin, *ACS Appl. Energy Mater.*, **1**, 2979 (2018); https://doi.org/10.1021/acsaem.8b00781
17. R. Pothu, R. Bolagam, Q. Wang, W. Ni, J. Cai, X. Peng, Y. Feng and J. Ma, *Rare Met.*, **40**, 353 (2021); https://doi.org/10.1007/s12598-020-01470-w
18. H.S. Jadhav, S.M. Pawar, A.H. Jadhav, G.M. Thorat and J.G. Seo, *Sci. Rep.*, **6**, 31120 (2016); https://doi.org/10.1038/srep31120
19. K.D. Kumar, N. Roy, T. Ramachandran, I.K. Durga, M.S. Khan, Y.A. Kumar and S.W. Joo, *Mater. Sci. Eng. B*, **306**, 117444 (2024); https://doi.org/10.1016/j.mseb.2024.117444
20. K.C. Babu Naidu and W. Madhuri, *Bull. Mater. Sci.*, **40**, 417 (2017); https://doi.org/10.1007/s12034-017-1374-4
21. R. Kashyap, R. Kumar, S. Devi, M. Kumar, S. Tyagi and D. Kumar, *Mater. Res. Express*, **6**, 125034 (2019); https://doi.org/10.1088/2053-1591/ab55b5
22. T. Vigneswari and P. Raji, *Int. J. Mater. Res.*, **109**, 413 (2018); https://doi.org/10.3139/146.111628
23. C. Ojha, *Int. J. Curr. Sci.*, **15**, 105 (2025).
24. M. Emek, E.İ. Şahin, J.E.F.M. Ibrahim and M. Kartal, *Nanomaterials*, **15**, 1580 (2025); https://doi.org/10.3390/nano15201580
25. I.F.F. Christopher and A. Karuppiah, *Chem. Phys. Impact*, **8**, 100460 (2024); https://doi.org/10.1016/j.chphi.2024.100460
26. T.M. Naidu and P.L. Narayana, *J. Nanosci. Technol.*, **5**, 769 (2019); https://doi.org/10.30799/jnst.247.19050407
27. M.A. Fathy, A.H. Kamel and S.S. Hassan, *RSC Adv.*, **12**, 7433 (2022); https://doi.org/10.1039/D2RA00034B
28. M.A. Iqubal, S.S. Islam, K. Ghosh, R.A. Molla, Kamaluddin and S.M. Islam, *J. Inorg. Organomet. Polym. Mater.*, **27**, 1730 (2017); https://doi.org/10.1007/s10904-017-0636-3
29. M. Hafeez, R. Shaheen, B. Akram, Zain-ul-Abdin, S. Haq, S. Mahsud, S. Ali and R.T. Khan, *Mater. Res. Express*, **7**, 025019 (2020); https://doi.org/10.1088/2053-1591/ab70dd
30. M.M. El-Masry and R. Ramadan, *Appl. Phys., A Mater. Sci. Process.*, **128**, 110 (2022); https://doi.org/10.1007/s00339-021-05238-6
31. A.N. Naveen and S. Selladurai, *Electrochim. Acta*, **125**, 404 (2014); https://doi.org/10.1016/j.electacta.2014.01.161
32. A.H. Bashal, K.D. Khalil, A.M. Abu-Dief and M.A. El-Atawy, *Chem. Adv. Mater.*, **3**, 67 (2018); https://doi.org/10.1016/j.ijbiomac.2023.126856
33. J. Zhang and Z.H. Chen, *Front. Mater.*, **7**, 178 (2020); https://doi.org/10.3389/fmats.2020.00178
34. B. Nandan, M.C. Bhatnagar and S.C. Kashyap, *J. Phys. Chem. Solids*, **129**, 298 (2019); https://doi.org/10.1016/j.jpcs.2019.01.017
35. S.B. Gopale, G.N. Kakade, G.D. Kulkarni, V. Vinayak, S.P. Jadhav and K.M. Jadhav, *J. Phys. Conf. Ser.*, **1644**, 012010 (2020); https://doi.org/10.1088/1742-6596/1644/1/012010
36. S.R. Shahina and S. Vidya, *AIP Conf. Proc.*, **2379**, 030012 (2021); https://doi.org/10.1063/5.0058235
37. M. Parishani, M. Nadafan, Z. Dehghani, R. Malekfar and G.H.H. Khorrami, *Results Phys.*, **7**, 3619 (2017); https://doi.org/10.1016/j.rinp.2017.09.049
38. D.D.M. Prabaharan, K. Sadaiyandi, M. Mahendran and S. Sagadevan, *Appl. Phys., A Mater. Sci. Process.*, **123**, 264 (2017); https://doi.org/10.1007/s00339-017-0786-8
39. C.L. Priyadharsini, G. Marimuthu, T. Pazhanivel, P.M. Anbarasan, V. Aroulmoji, V. Siva and L. Mohana, *J. Sol-Gel Sci. Technol.*, **96**, 416 (2020); https://doi.org/10.1007/s10971-020-05393-x
40. S. Sagadevan, Z.Z. Chowdhury and R.F. Rafique, *Mater. Res.*, **21**, (2018); https://doi.org/10.1590/1980-5373-mr-2016-0533
41. Z. Mahhouti, H. El Moussaoui, T. Mahfoud, M. Hamedoun, M. El Marssi, A. Lahmar, A. El Kenz and A. Benyoussef, *J. Mater. Sci. Mater. Electron.*, **30**, 14913 (2019); https://doi.org/10.1007/s10854-019-01863-3
42. A.A. Ati, *J. Mater. Sci. Mater. Electron.*, **29**, 12010 (2018); https://doi.org/10.1007/s10854-018-9305-8
43. S. Sagadevan, J. Podder and I. Das, in eds.: J. Ebenezar, Springer Proceedings in Physics, Cham, Switzerland: Springer, vol. 189, pp. 145-152 (2017).
44. N. Elgrishi, K.J. Rountree, B.D. McCarthy, E.S. Rountree, T.T. Eisenhart and J.L. Dempsey, *J. Chem. Educ.*, **95**, 197 (2018); https://doi.org/10.1021/acs.jchemed.7b00361
45. T.S. Mathis, N. Kurra, X. Wang, D. Pinto, P. Simon and Y. Gogotsi, *Adv. Energy Mater.*, **9**, 1902007 (2019); https://doi.org/10.1002/aenm.201902007
46. M.I.A. Abdel Maksoud, R.A. Fahim, A.E. Shalan, M. Abd Elkodous, S.O. Olojede, A.I. Osman, C. Farrell, A.A.H. Al-Muhtaseb, A.S. Awed, A.H. Ashour and D.W. Rooney, *Environ. Chem. Lett.*, **19**, 375 (2021); https://doi.org/10.1007/s10311-020-01075-w
47. H. Hitha, S. Kuriakose, F. Xavier, S.K. Stephen, M. John and T. Varghese, *Mater. Today Proc.*, (2023); https://doi.org/10.1016/j.matpr.2023.11.144
48. S. Debnath, A. Das and R. Das, *Ceram. Int.*, **47**, 16467 (2021); https://doi.org/10.1016/j.ceramint.2021.02.095
49. N.C. Joshi, P. Gururani, S. Chetana and N. Kumar, *J. Inorg. Organomet. Polym. Mater.*, **33**, 1909 (2023); https://doi.org/10.1007/s10904-023-02631-x
50. N.C. Joshi, P. Gururani and N. Kumar, *Ionics*, **30**, 6531 (2024); https://doi.org/10.1007/s11581-024-05742-8
51. S. Sharifi, A. Yazdani and K. Rahimi, *Mater. Sci. Semicond. Process.*, **108**, 104902 (2020); https://doi.org/10.1016/j.mssp.2019.104902
52. N.M. Malima, M.D. Khan, J. Choi, R.K. Gupta, P. Mashazi, T. Nyokong and N. Revaprasadu, *RSC Adv.*, **11**, 31002 (2021); https://doi.org/10.1039/D1RA04833C
53. S.A. Al Kiey, M.M. Ahmad and A.A. Azab, *J. Energy Storage*, **148**, 119968 (2026); https://doi.org/10.1016/j.est.2025.119968
54. N.C. Joshi, P. Gururani and S. Kimothi, *Inorg. Chem. Commun.*, **153**, 110786 (2023); https://doi.org/10.1016/j.inoche.2023.110786